# Calculation of nuclear reaction cross sections on excited nuclei with the coupled-channels method

T. Kawano,* P. Talou, J. E. Lynn, M. B. Chadwick, and D. G. Madland
*Theoretical Division, Los Alamos National Laboratory, Los Alamos, New Mexico 87545, USA*
(Received 21 July 2009; published 31 June 2009)

We calculate nuclear cross sections on excited nuclei in the fast neutron energy range. We partition the whole process into two contributions: the direct reaction part and the compound nuclear reactions. A coupled-channels method is used for calculating the direct transition of the nucleus from the initial excited state, which is a member of the ground-state rotational band, to the final ground and excited low-lying levels. This process is strongly affected by the channel coupling. The compound nuclear reactions on the excited state are calculated with the statistical Hauser-Feshbach model, with the transmission coefficients obtained from the coupled-channels calculation. The calculations are performed for a strongly deformed nucleus $^{169}$Tm, and selected cross sections for the ground and first excited states are compared. The calculation is also made for actinides to investigate possible modification to the fission cross section when the target is excited. It is shown that both the level coupling for the entrance channel, and the different target spin, change the fission cross section.

DOI: 10.1103/PhysRevC.80.024611 PACS number(s): 24.10.Eq, 24.50.+g, 24.60.Dr

## I. INTRODUCTION

Understanding nuclear reactions on excited nuclei is of physical interest for studying nucleosynthesis in nuclear astrophysics. Nuclear reaction rates for astrophysical applications are corrected by the stellar enhancement factor (SEF) [1], taking account of the thermal excitation of the target [2]. In a natural environment nuclear reactions normally take place on stable nuclei, with the target nucleus in its ground state or isomeric state. In the case of shape and spin isomers, because the excited state hardly couples to the ground state, they can be treated as if the target was in a ground state, but with a straightforward modification to the reaction $Q$ value. The excitation energy of the isomers is released by impinging neutrons, for example, via a compound nucleus reaction. It is sometimes referred to as a superelastic process [3,4], because the outgoing neutron is accelerated.

In a high-density high-temperature neutron and $\gamma$-ray environment, such as neutron stars or supernovae, it is likely that neutron-induced nuclear reactions occur on the excited states, even though the lifetime of the excited state is often in the order of a nanosecond or shorter. For example, the half-life of the first excited state of $^{169}$Tm is 4.08 ns, and that for $^{239}$Pu is 36 ps [5]. The nuclear reaction rates on the excited state could be different from those on the ground state, primarily because of the difference in phase space of levels accessible: the spin and parity of the ground and excited states usually differ, and the target excitation energy shifts the excitation energy of the compound system. This process can be calculated with a standard Hauser-Feshbach model [6] with an additional excitation energy on the target nucleus.

When a target nucleus is strongly deformed, we observe a rotational spectrum on each $K$ band, and this modifies the accessible phase space depending on which target state is excited. In the case where the excited target is a member of the ground-state rotational band, a direct reaction caused by an incident neutron can de-excite the target without forming a compound nucleus. In this direct inelastic scattering, the incoming neutron gains energy during the process. The direct reaction also may change the compound nuclear reaction process, because the total compound formation cross section and corresponding transmission coefficients differ if the target nucleus is in an excited state.

We study the nuclear reactions on the excited nuclei in the framework of the coupled-channels (CC) formalism [7,8]. The direct cross sections for the ground or excited states are calculated by solving the coupled Schrödinger equations, and transmission coefficients for both ground and excited states are obtained from the same scattering ($S$) matrix elements, using a symmetry property of the $S$ matrix. We calculate nuclear reactions on $^{169}$Tm, because of properties that simplify our calculations: there are precedent studies by Madland [9], and Madland and Doolen [10], the target is well deformed ($\beta_2 = 0.3$) [11], it does not fission by a fast energy neutron, and charged particle emission channels can be ignored. The calculations for $^{169}$Tm are performed at low energies [below the $(n,2n)$ reaction threshold energy], where we expect a constraint effect of target spin and partial wave angular momentum couplings. We also perform studies of the fission cross sections of $^{239}$Pu using the Hauser-Feshbach model that includes multiple-chance fission in the higher-energy range.

The excited nuclei at low-lying states are produced in various way, e.g., by neutron inelastic scattering, $\gamma$ ray absorption, neutron radiative capture, inverse internal conversion, and so on. For example, the nuclear reaction process during ICF (inertial confinement fusion) may involve neutron interactions on the excited nuclei. It should be emphasized that measurements of nuclear reaction cross sections on very short-lived targets are extremely difficult, or impossible, within an acceptable uncertainty, so that prediction of these cross sections by model calculations is essential. The method described in this study is general, and it can be applied to any medium/heavy nucleus whenever knowledge of nuclear reactions on the excited target is crucial in applications. This may provide some insight on possible modifications to the

*kawano@lanl.gov

 

nuclear reaction rates on important waiting point nuclei in nucleosynthesis.

## II. THEORY

### A. Direct nuclear reaction

The formulation of the CC method is given in Refs. [7,8]. Solving a set of coupled equations gives a scattering matrix element $S_{cc'}^{J\Pi}$, where the channel $c$ is specified by quantum numbers of the incoming/outgoing wave $(l, s, j)$, $J\Pi$ the total spin and parity, and the target state $n$ that designates the spin $I_n$ and parity $\pi_n$. $n = 0$ stands for the ground state, $n = 1$ is for the first excited state, the quantities with a prime are for the exit channel, and so on.

We limit ourselves to consider neutron-induced reactions. Because the scattering matrix element $S_{cc'}^{J\Pi}$ is symmetric, the direct cross sections from any $n$-th level can be calculated by

$$\sigma_R^{(n)} = \frac{\pi}{k_n^2} \sum_{J\Pi} \sum_c \delta_{n_c,n} g_J \left(1 - \sum_{c'} \left|S_{cc'}^{J\Pi}\right|^2\right), \quad (1)$$

$$\sigma_D^{(nn')} = \frac{\pi}{k_n^2} \sum_{J\Pi} \sum_c \delta_{n_c,n} g_J \sum_{c'} \left|\delta_{cc'} - S_{cc'}^{J\Pi}\right|^2 \delta_{n_{c'},n'}, \quad (2)$$

where $g_J$ is the spin factor given by

$$g_J = \frac{2J+1}{(2s+1)(2I_n+1)}, \quad (3)$$

where $s$ is the intrinsic spin of neutron, $k_n$ is the incoming wave number, $n_c$ is the index of the excited level to which the channel $c$ belongs, $\sigma_R^{(n)}$ is the reaction (compound formation) cross section when the target is at the $n$-th level, and $\sigma_D^{(nn')}$ is the direct inelastic-scattering cross section from the $n$-th to the $n'$-th level. For a special case, $n = n'$ is for the shape elastic scattering $\sigma_E^{(n)}$. The total cross section $\sigma_T^{(n)}$ can be expressed in terms of the $S$-matrix elements, or more conveniently,

$$\sigma_T^{(n)} = \sigma_R^{(n)} + \sum_{n'} \sigma_D^{(nn')}. \quad (4)$$

Figure 1 shows a scheme of CC calculation for the ground-state rotational band $[(1/2)^+$-$(3/2)^+$-$(5/2)^+$-$(7/2)^+]$,

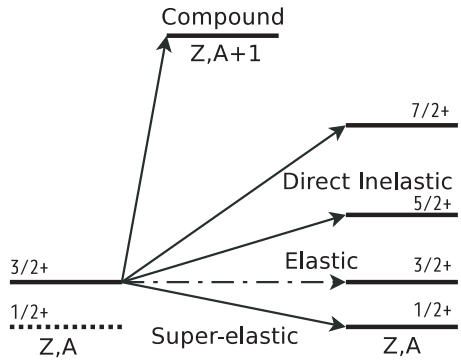


FIG. 1. An example of coupled-channels calculation for the excited state. The target is at the first $(3/2)^+$ state, which is a member of ground-state rotational band. The coupled equations give a set of direct cross sections and the compound formation cross section. In this case the direct transition to the $(3/2)^+$ level is elastic scattering and to other levels is inelastic scattering.

when the target is at the $(3/2)^+$ level. In this case the elastic scattering is a direct transition to the first excited $(3/2)^+$ level. The direct process to the ground state $(1/2)^+$ is one of the inelastic-scattering channels, although the outgoing neutron energy becomes higher than the incident neutron energy, which is often called superelastic (or sometimes superinelastic). In this article we regard this as one of the inelastic-scattering process. Not only the direct reaction but also the compound process to the ground state, $A^* + n \to (A+1)^* \to A + n'$, releases the target excitation energy too.

As the reaction cross section $\sigma_R$ is calculated in Eq. (1), the generalized transmission coefficient $T_{lj}^{(n)}$, which is defined as the probability of formation of compound nucleus on the $n$-th state by a neutron having the orbital angular momentum and spin of $l$, $j$, is given by

$$T_{lj}^{(n)} = \sum_{J\Pi} \sum_c \frac{2s+1}{2j_c+1} g_J \left(1 - \sum_{c'} \left|S_{cc'}^{J\Pi}\right|^2\right) \delta_{n_c,n} \delta_{l_c,l} \delta_{j_c,j}, \quad (5)$$

where $\delta_{l_c,l}$ is the Kronecker delta. Equation (5) gives a partial-wave contribution to the total reaction cross section as

$$\sigma_R^{(n)} = \frac{\pi}{k_n^2} \sum_{lj} \frac{2j+1}{2s+1} T_{lj}^{(n)}. \quad (6)$$

The transmission coefficient in Eq. (5) is the one we can use in the Hauser-Feshbach model. In many previous calculations $T_{lj}$ in the Hauser-Feshbach model is calculated for the ground state, and the decay channel transmission coefficients $T_{lj}^{(n)}$ are replaced by the ground state $T_{lj}^{(0)}$ calculated at a shifted energy, $T_{lj}^{(n)}(E) = T_{lj}^{(0)}(E - E_x)$. Because our method gives a correct $T_{lj}^{(n)}$ for all excited states, such an approximation is not involved in our Hauser-Feshbach calculations.

### B. Compound nuclear reaction

The Hauser-Feshbach theory [6] needs to be modified when the number of open channels is small [12]. This width fluctuation correction has been studied for the spherical nucleus case [13–16]. Two independent computational studies of Igarasi [17] and Hilaire, Lagrange, and Koning [18] showed that the integration method with Monte Carlo simulation for the channel degree-of-freedom $\nu$ by Moldauer [14] gives almost an identical result to the most exact solution by Verbaarschot *et al.* of the energy-averaged $S$-matrix element using the Gaussian orthogonal ensemble (GOE) [16].

Kawai, Kerman, and McVoy (KKM) [19] formulated the compound nuclear reaction in terms of the CC method, in which the nuclear deformation is automatically taken into account. In KKM, the generalized transmission coefficient in Eq. (5) is not used, but the compound cross section is defined in terms of a penetration matrix $P$, which is calculated from the $S$ matrix as [20]

$$P_{cc'} = \delta_{cc'} - \sum_{c''} S_{cc''} S_{c''c'}^*. \quad (7)$$

Other techniques deal with the direct channels in the compound reaction by a unitary transformation (Engelbrecht-Weidenmüller transformation) [21,22] to diagonalize the $S$ matrix. A method of Nishioka, Weidenmüller, and Yoshida [23] is a natural extension of the GOE triple integral to the penetration matrix, which is, however, not practical for numerical calculations. We have shown [24] that the KKM theory gives very similar cross sections to that of Moldauer's method, and we do not expect a large modification to the calculated result because this is a correction to the width fluctuation correction factor (inclusion of direct channel, which is typically about ∼5–10% contribution to the total scattering.) Therefore, in this study, the compound cross section is not calculated from Eq. (7), but the spin-averaged form in Eq. (5).

In our calculations, therefore, the width fluctuation correction to the Hauser-Feshbach theory is calculated by the Moldauer's method [14], using the generalized transmission coefficient in Eq. (5). This is a so-called detailed balance calculation [7]. The systematics of $\nu$ are replaced by a recent study of Ernebjerg and Herman [25], which better reproduces the GOE calculations. When the target is in an excited state, the width fluctuation elastic enhancement occurs for the excited state. This method has been applied to calculate neutron radiative capture cross sections on actinides [26,27], and it was shown that the calculated capture cross sections on $^{237}$Np and $^{241}$Am well reproduce the experimental data from Los Alamos.

As schematically shown in Fig. 2 all the transmission coefficients for the compound nucleus decay channels are easily obtained by the CC calculation with the detailed balance technique. For example, the transmission coefficient from the compound nucleus to the excited $(3/2)^+$ state (exit channel) is identical to that of compound formation probability (entrance channel). A transmission coefficient to uncoupled states (shown by the dotted arrow in Fig. 2) is given by solving a spherical optical model on this excited state, which forms the same compound state as the entrance channel. The optical

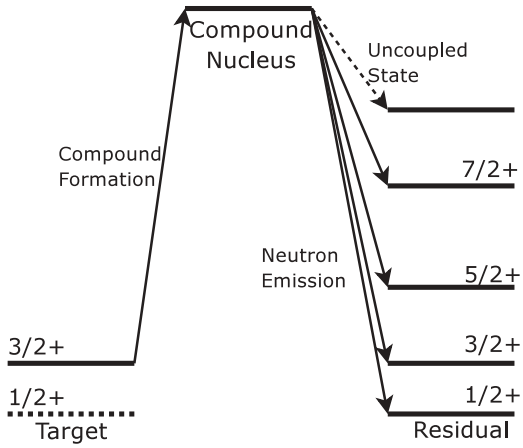


FIG. 2. Transmission coefficients used in the Hauser-Feshbach calculation. The transmission coefficients for the rotational band members are obtained by the CC calculation. For the uncoupled state, we perform a spherical optical model calculation.

potential for these spherical calculations would be different from that for the CC calculation. Indeed, it is possible to increase the imaginary potential phenomenologically or apply a global spherical optical potential for those uncoupled states to account for eliminating the direct channels in the CC calculation. In this study we simply adopt the same optical potential parameters of the CC model for the uncoupled states and perform spherical optical model calculations. The same procedure is used both for calculations of targets in their ground state and in their excited states.

## III. RESULTS AND DISCUSSION

### A. Coupled-channels calculation for $^{169}$Tm

The CC optical potential parameter for $^{169}$Tm was taken from Ref. [9]: they are

$$V = 46.87 - 0.25\,E \text{ MeV}, \tag{8}$$

$$W_s = 3.6 + 0.6\,E \text{ MeV}, \tag{9}$$

$$V_{\rm so} = 6.0 \text{ MeV}, \tag{10}$$

where $V$ is the Wood-Saxon central potential depth, $W_s$ is the derivative Woods-Saxon imaginary potential, $V_{\rm so}$ is the Thomas-type spin-orbit potential, and $E$ is the incident neutron energy in MeV. The radius $r$ and diffuseness $a$ for each potential are $r_v = r_w = r_{\rm so} = 1.27$ fm, $a_v = a_{\rm so} = 0.63$ fm, and $a_w = 0.48$ fm, in common notation. The deformation parameters of $^{169}$Tm are $\beta_2 = 0.31$ and $\beta_4 = -0.01$. We coupled five levels of the ground-state rotational band, $(1/2)^+$, $(3/2)^+$, $(5/2)^+$, $(7/2)^+$, and $(9/2)^+$, and calculated the direct cross sections for two cases: (1) the target is in the ground state and (2) the target is in the first excited state, $(3/2)^+8.41$ keV. The neutron incident energies considered are from 1 keV up to 20 MeV, but we are mostly interested in the low-energy region. We expect noticeable differences in the calculated cross sections at low energies, because the number of incoming partial waves is not so large, which limits the accessible spin-space in the reaction and amplifies the calculated differences for the target in its ground state versus excited states.

The calculated total, shape elastic, and reaction (compound formation) cross sections are shown in Fig. 3. The thick lines are the calculated results when the target is in the ground state, and the thin lines are for the first excited state case. Differences are clearly observed in the low-energy region, as we expected. At 1 keV, $\sigma_R^{(1)}/\sigma_R^{(0)}$ is 1.33 and $\sigma_E^{(1)}/\sigma_E^{(0)}$ are about 0.77. The increase in $\sigma_R$ at low energies is due to the $s$-wave transmission coefficient, and therefore can be related to the $s$-wave strength function. The calculated $S_0$ for the ground state and first excited cases are $1.81 \times 10^{-4}$ and $2.44 \times 10^{-4}$, respectively. However, the $p$-wave strength function $S_1$ for both cases are not so different (less than 5% difference).

Above 5 MeV or so, differences in these cross sections become very small, and this is expected because the excitation energy of the first level is only 8.41 keV, which is only 0.1% of the incident energies. In addition, there are many partial waves that couple to the total $J\Pi$, which washes out the difference in the target spin (which is only $1\hbar$ anyway).

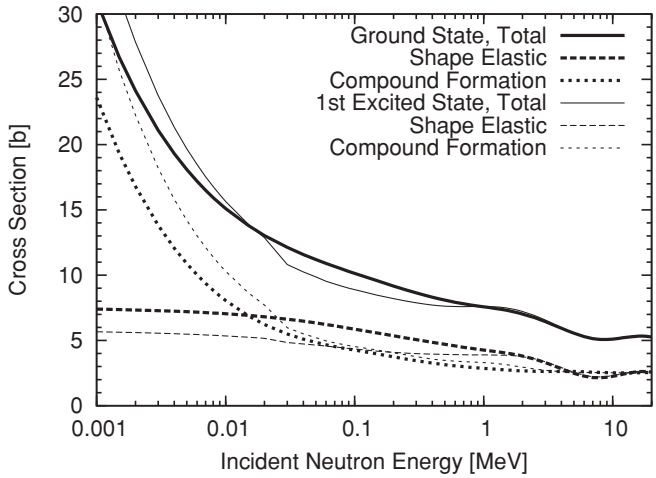


FIG. 3. Calculated total (solid line), shape elastic scattering (dashed line), and reaction cross sections (dotted line) for $^{169}$Tm. The thick lines are for the ground-state case, and thin lines are for the first excited state.

The target spin effect appears only in the CC model, because spherical optical model (SOM) calculations are target spin independent. In the SOM case, the transmission coefficients on the excited states are calculated regardless of the $I^\pi$ of the state. Note that this implies that the same spherical optical potential obtained for the ground-state target can be applied to the excited states, although there might be a nonoverlapped phase space; compound states that satisfy the spin selection rule $|I - j| \leqslant J \leqslant I + j$ are different.

The direct cross sections are depicted in Fig. 4. The thick curves are the usual CC calculations, in which the target is at the ground state. Our unique calculation is the direct

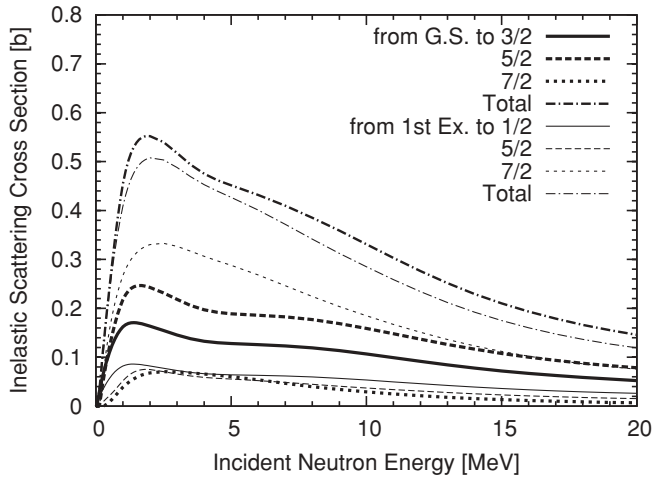


FIG. 4. Calculated direct inelastic scattering cross sections for two cases; target at the ground state (thick curves), and at the first excited state (thin curves). Although we coupled the $(9/2)^+$ state too, the cross sections are not plotted here for clearer visibility. For the ground state case, the solid line is the direct cross section to the $(3/2)^+$ state. In the case of excited target, the solid line is the direct cross section to the $(1/2)^+$ ground state. The dot-dashed curves are the sum of all direct reactions.

TABLE I. Nmerical comparison of the calculated cross sections for the target in its ground state $(1/2)^+$ and in its first excited state $(3/2)^+$ at the neutron incident energy of 100 keV, with those by Madland [9]. The cross sections are in barns.

| | Present | | Madland [9] | |
|---|---|---|---|---|
| | $(1/2)^+$ | $(3/2)^+$ | $(1/2)^+$ | $(3/2)^+$ |
| Total | 10.1 | 8.89 | 10.3 | 8.98 |
| Shape elastic | 5.86 | 4.34 | 5.91 | 4.45 |
| Compound formation | 4.26 | 4.53 | 4.35 | 4.52 |
| Total inelastic | 1.03 | 0.569 | 1.17 | 0.650 |
| Capture | 0.625 | 0.852 | 0.625 | 0.941 |

transition from the first excited $(3/2)^+$ state to the ground state, shown by the thin solid curve. This process has a positive $Q$ value, which means the scattered neutrons are accelerated. This cross section is a factor of 2 smaller than the normal process: from the ground state to the first excited state (thick solid curve). However, the inelastic scattering to the $(7/2)^+$ state is significantly enhanced. It is interesting to note that the sum of all direct inelastic scattering cross sections, shown by the dot-dashed curve, are not so different. Although we see 20% difference in the total inelastic-scattering cross section at 20 MeV, this is only 1% of the total reaction cross section.

The direct cross section from the $(3/2)^+$ state to the ground state is about a half of the cross section from the ground state to the $(3/2)^+$ excited state, and this is the same ratio as $(2I_0 + 1)/(2I_1 + 1)$. This is related to the spin-factor of Eq. (3). Because the $S$-matrix is symmetric whichever the incident particle channel is in, the difference in the direct cross section $\sigma_D^{(nn')}$ comes from $g_J$ and a channel selection $\delta_{n_c,n}$ and $\delta_{n_{c'},n'}$ in summation in Eq. (2), and the simplest case is just equal to the ratio of $g_J$'s. In addition, differences also occur because we adopted the energy-dependent optical potential parameters of Eqs. (8)–(10).

We also compared the present results numerically with the independent calculations in Ref. [9]. Table I shows the calculated cross sections at 100 keV. The table shows that the two independent solutions for the ground- and excited-state scattering cross sections yield essentially the same results, and this gives credence to the approach.

### B. Statistical model calculation for $^{169}$Tm

#### *1. Neutron radiative capture*

The calculated transmission coefficients of Eq. (5) are fed to the statistical Hauser-Feshbach-Moldauer model calculations. The CC calculation for the entrance channel is performed by coupling the five ground-state rotational band members [up to 332 keV $(9/2)^+$ level]. Discrete levels are included up to 938 keV $(13/2)^-$ level, and their spin and parity are taken from the reference input parameter library version 2, RIPL-2 [28]. Above 938 keV, the Gilbert-Cameron level-density formulas [29] with a parameter systematics in Ref. [30] are employed. There is a 316-keV $(7/2)^+$ level, whose excitation energy is lower than the 332-keV $(9/2)^+$ level. We included this level as an uncoupled state in the Hauser-Feshbach model calculation.

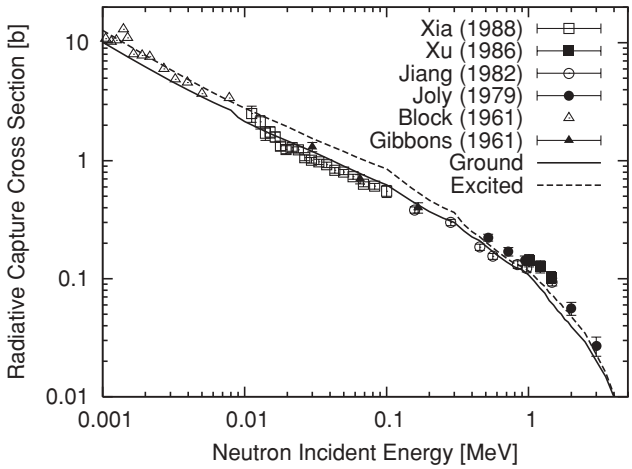


FIG. 5. Comparison of calculated neutron radiative capture cross section with experimental data. The solid curve is for the ground state case, and the dashed curve is for the excited state. All the experimental data are for the ground state.

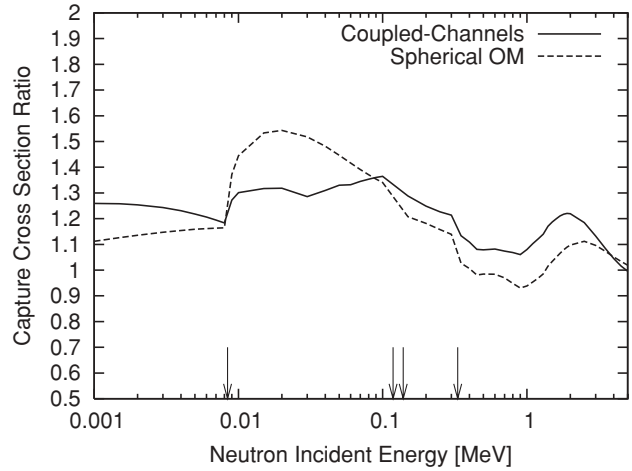


FIG. 6. Ratios of the calculated capture cross sections of excited state to the ground state. The solid line is for the coupled-channels calculation, and the dashed line is for the spherical optical model case. The arrows on the x axis are the inelastic channel threshold energies.

The E1 $\gamma$-ray strength function for the radiative capture channel is calculated with the generalized Lorentzian form [31], with the giant dipole resonance parameter in Ref. [28]. For higher multipole radiations, we include E2 and M1 transitions. The $\gamma$-ray strength function is then renormalized to the complied $\langle\Gamma_\gamma\rangle/D_0$ value taken to be 0.0118 [32]. This normalization factor for the $\gamma$-ray strength function must be obtained for the ground state, because the $\langle\Gamma_\gamma\rangle/D_0$ value is for the ground state. Then, of course the same normalization factor is applied for the excited state cases, because we assume that a giant-dipole state on the excited state is the same as on the ground state by the Brink-Axel hypothesis.

The calculation is performed up to the neutron incident energy of 8 MeV. At higher energies, the dominant neutron capture reaction becomes the direct/semidirect process [33] that requires a target state wave function. Anyway we do not expect a large difference in the calculated cross sections for both cases at high energies, because the total reaction cross sections $\sigma_R^{(0)}$ and $\sigma_R^{(1)}$ are almost the same.

Comparison of the calculated neutron capture cross section with the experimental data are shown in Fig. 5. The solid line is a calculation when the target is in its ground state, and the dashed line is for the first excited state case, respectively. The numerical comparison with the results in Ref. [9] is also shown in Table I. The ground-state calculation is compared with the experimental data available [34–38]. Agreement between the ground-state calculation and the experimental data is seen and it is fairly good, though in this figure we are more focused on a prediction of differences between ground state and excited state capture. The shape of the calculated capture cross sections on both states are very similar, but the absolute magnitudes differ by 20–30% below 100 keV. One of the reasons of this difference is the compound formation cross sections, which are different for both cases as shown in Fig. 3. However, the differences between $\sigma_R^{(0)}$ and $\sigma_R^{(1)}$ are visible only below 100 keV. Another reason could be a difference in the total spin of the compound nucleus. Assuming the incoming partial wave is just an $s$-wave, the spin of compound state is $I \pm 1/2$, and this gives a different $\gamma$-ray cascading pattern from the compound state and different competition of neutron emission processes.

When an SOM calculation to the entrance channels is employed, the compound formation cross section does not depend on the target spin (however, the spin distribution of the compound nucleus is still different). To see the effect of channel coupling, we also performed the neutron capture calculation with the spherical optical model (SOM) potential. The global optical potential parameters of Koning and Delaroche [39] were used. Figure 6 shows a ratio of the calculated capture cross sections on the excited state to the ground state. Because the shape of both curves are similar above 100 keV, the enhancement of the capture cross sections in the energy range 100 keV to 1 MeV is probably due to the target spin effect. At low energies CC and SOM calculations give somewhat different tendencies. The SOM calculation enhances the capture cross section significantly from 10 to 100 keV. Although an old-fashioned spherical optical model and Hauser-Feshbach model gives the same compound formation cross section, there would still be an enhancement to the capture cross section, because of $J\Pi$ coupling.

#### *2. Neutron elastic and inelastic scattering*

The calculated neutron elastic-scattering cross section is shown in Fig. 7. The dashed lines are the shape elastic scattering, which are identical to those in Fig. 3. The dot-dashed lines are the compound elastic, and the solid line is the total elastic-scattering cross sections. For the excited target case, reduction in the shape elastic scattering $\sigma_E^{(1)}$, having the similar total cross sections for both cases, results in an increase in the compound formation $\sigma_R^{(1)}$, which enhances the compound elastic-scattering cross section [$\sigma_R^{(1)}$ is the sum of the compound elastic and neutron capture below 8.41 keV].

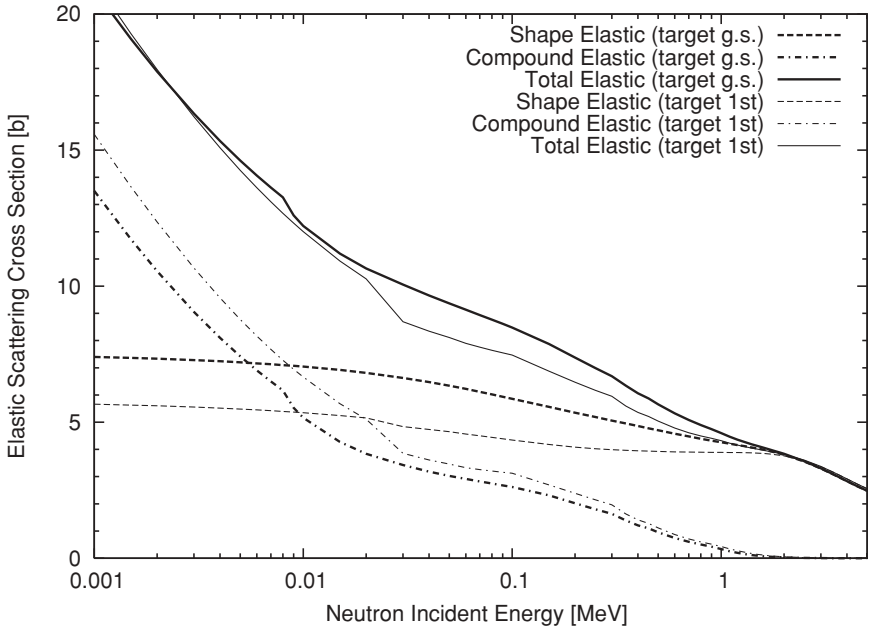


FIG. 7. Comparison of calculated neutron elastic-scattering cross sections. The thick lines are for the ground-state target, and the thin lines are for the excited state. The solid lines are the total inelastic-scattering cross sections, dashed lines are the shape elastic, and dot-dashed lines are the compound elastic scattering.

The total elastic-scattering cross sections look identical below 10 keV. This is, however, probably a coincidence, because the total elastic scattering at low energies depends on how large the neutron capture competition is. Above 2 MeV the compound elastic-scattering cross section becomes negligible, because many neutron inelastic-scattering channels open.

The calculated neutron inelastic-scattering cross sections, including both the direct and compound processes, are shown in Fig. 8. The thick solid line is the total inelastic scattering, which is a threshold reaction. The thin solid line is the result for the excited target with a negative $Q$ value. The dashed and dot-dashed lines are the production cross section of the 8.41- and 118-keV levels, respectively. The compound cross sections to the higher energy levels (above 118-keV levels) become similar for both cases, because a large phase space (many partial waves and large numbers of spin couplings) washes out the spin selection rule that is important when only a few partial waves are involved.

One obvious difference seen in Fig. 8 is, of course, the transition from the excited state to the ground state, which has no threshold. The superelastic cross section is, however, only 15% of the total elastic scattering (see Fig. 7). To observe the superelastically scattered neutrons, very high resolution experiments would be needed.

### C. Fission calculation for $^{239}$Pu

In the case of actinides, the low-incident neutron energy regime is dominated by capture and fission reaction processes. At relatively low neutron energies, the fission cross section is

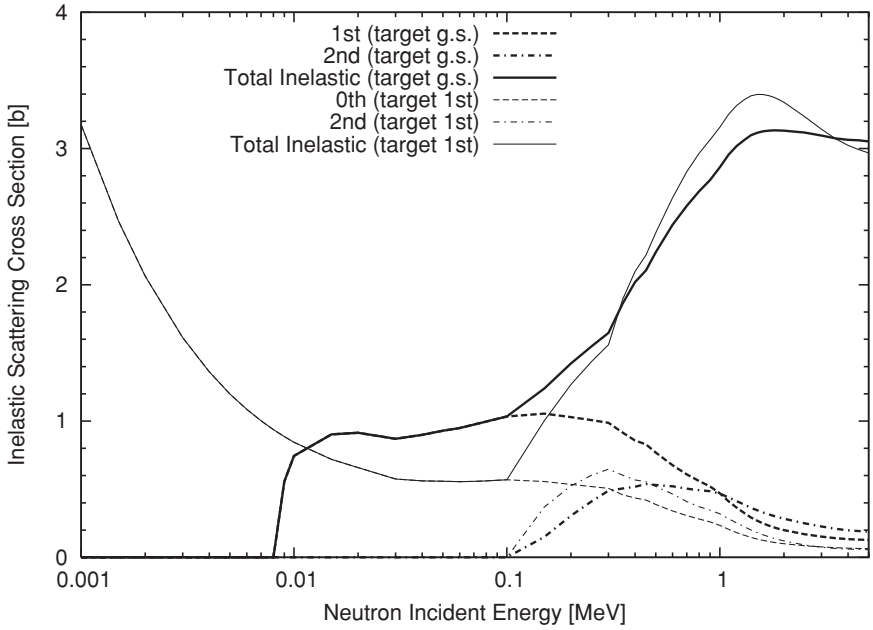


FIG. 8. Comparison of calculated neutron inelastic-scattering cross sections. The thick lines are for the ground state target, and the thin lines are for the excited state. The solid lines are the total inelastic-scattering cross sections.

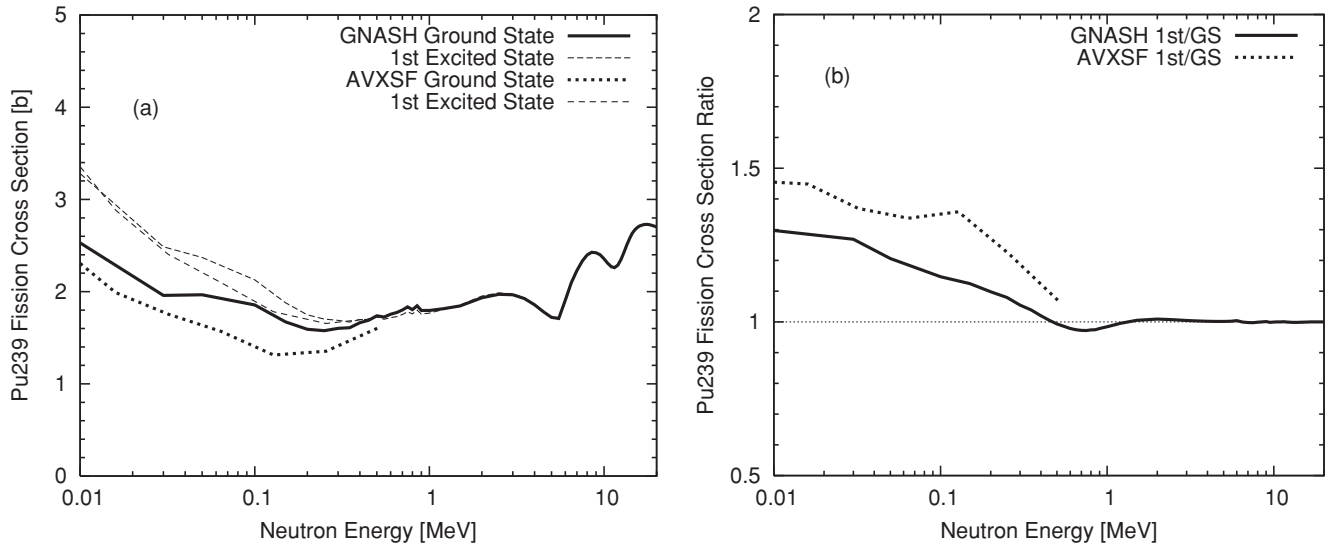


FIG. 9. (a) The neutron-induced fission cross section of $^{239}$Pu calculated in the two cases where the target nucleus is in its first excited state versus in its ground state; (b) the ratio of fission cross section for excited $^{239}$Pu to the ground-state target.

dominated by a relatively few transition states at the barrier deformations. In particular, the compound nucleus $^{240}$Pu is believed, from experimental evidence on shape isomers and theoretical calculations of energy as a function of deformation, to have a higher inner barrier peak than outer. Its fission probability in a state of given total angular momentum and parity is therefore strongly affected by the small number of transition states below the pairing energy gap at the inner barrier. A change in the spin and parity of the target nucleus, and hence of the compound nucleus, can have a significant impact on the fission cross section.

We have investigated this question by calculating the neutron induced fission cross section on $^{239}$Pu, either in its ground state [$I^\pi = (1/2)^+$] or in its first excited state [$E_x =$ 7.86 keV; $I^\pi = (3/2)^+$]. The coupled-channels calculations was performed using the optical potential of P. G. Young [28,40] and considering the first five states of the ground-state rotational band.

We have performed Hauser-Feshbach calculations using the GNASH code [41] and more detailed fission cross-section calculations using the AVXSF code by J. E. Lynn [42,43]. Because these two codes have different specialities, comparing two results may reduce code-specific problems in the fission calculations within the Hauser-Feshbach formalism. The modeling of the fission channel in GNASH is not particularly well suited for calculating the fission cross section below the barrier, as the coupling between class I and class II states is neglected. We also neglected the width fluctuation correction to the GNASH calculation. Better fission physics has been implemented in the AVXSF code, including correct treatments of the class I and class II states coupling. However, the neutron transmission coefficients are calculated from the experimental neutron strength function, and they are assumed to be the same for both the ground and excited states. However, GNASH employs the coupled-channels transmission coefficients.

Before we performed the Hauser-Feshbach calculations, we compared the reaction cross sections $\sigma_R$ calculated with the coupled-channels method, just as in Fig. 3. It was observed that these cross sections for both cases are very similar, except that we saw an increase in $\sigma_R$ for the first excited state. This might be due to the optical potential employed. At least we could say here that the comparison of fission calculation may reveal the target spin dependence of the fission process. An assumption made in the AVXSF calculation is that the same neutron strength function is used for both ground and excited states, and this is supported by the coupled-channels calculation.

Figure 9 shows the calculated fission cross section in the two situations, with two different codes. Two thick curves are for the ground-state case; the solid curve is with GNASH and the dotted curve is with AVXSF. Other thin curves are for the excited state case; the dashed curve is for GNASH, and the dot-dashed curve is for AVXSF. Note that the AVXSF calculations go up to 500 keV. Both codes indicate that the calculated fission cross sections are enhanced when the target is in its excited state. The cross section ratios of the excited to the ground states are shown in the lower panel of Fig. 9. Although the absolute magnitude of the enhancement is different in GNASH and AVXSF, their tendency is very similar, and the fact that both calculations lead to the same qualitative conclusion is comforting and indicates that the underlying physics of the transition states is correct.

At 10 keV the calculated first excited-state cross section with GNASH is about 30% higher than the ground-state cross section. This enhancement becomes 50% for the case of AVXSF. We understand that the enhancement reflects the different spin of the target state [$(3/2)^+$ for the first excited state and $(1/2)^+$ for the ground state], which modifies possible fission paths through the discrete transition states lying on top of the barriers. At low energies a few partial waves contribute to the compound formation, and decay of the compound nucleus is strongly constrained by the spin selection rule.

For example, the $s$-wave coupled with the ground state of the target nucleus produces the compound nucleus states of $0^+$ (with spin statistical weighting of 1/4) and $1^+$ (with spin statistical weighting of 3/4), whereas two spin states $1^+$ and $2^+$ (with respective weightings of 3/8 and 5/8) are possible in the case of the $I^\pi = 3/2^+$ excited state. The $1^+$ transition state at the inner barrier plays a special role as it is expected to lie much higher in excitation energy than other spin-parity states, due to its intrinsic complexity (e.g., a combination of bending and mass-asymmetry vibrations). Therefore the fission cross section observed for the $^{239}$Pu in its ground state is hindered compared to the one for the first excited state. In the AVXSF calculation the class II intermediate structure associated with the $1^+$ state has the effect of further reducing the average fission cross section, and this could explain the higher ratio of excited state to ground state cross sections shown in Fig. 9

Above 1 MeV neutron incident energy, the two results with GNASH are practically identical because the number of incoming partial waves becomes large, then the available phase spaces for both cases get very similar.

With the AVXSF code, we performed more fission cross section calculations for the cases in which the target nucleus is in the higher excited states, not only the ground state rotational band, but also $K = (5/2)^+$ band members whose bandhead energy is 285 keV. Because the angular-momentum conservation during the fission process is not well understood ($K$ mixing [42]), a quantitative argument requires more detailed information of nuclear structure for strongly deformed systems. However, qualitatively the calculated fission cross section is larger than that for the ground state, and this enhancement tends to be larger if the target spin is higher.

## IV. CONCLUSION

We have applied a CC method to calculate nuclear reaction cross sections for excited nuclei. The direct reactions among the members of ground-state rotational band are calculated with the CC method, and the generalized transmission coefficients from both ground and excited states are calculated. These transmission coefficients are fed to the statistical Hauser-Feshbach model calculation to obtain compound reaction cross sections.

We performed a numerical comparison of cross sections for $^{169}$Tm. The statistical model calculation on the excited nucleus gives different cross sections from the calculation for the ground state. However, the differences are visible only below neutron energies of about 1 MeV. The difference of the cross sections comes from both the level coupling effect and the target spin effect. It was shown that the target spin effect is important, when a number of contributing partial waves is not so large. The level coupling effect is also important, which was shown by comparing with the spherical model calculation. Our results have confirmed the original excited-state calculations of Ref. [9].

The same technique is also applied to calculate fission cross sections of $^{239}$Pu, as the level structure of $^{239}$Pu is very similar to $^{169}$Tm. To reduce ambiguities in fission modeling in the Hauser-Feshbach framework, we employed two independent nuclear reaction model codes, GNASH and AVXSF. These two codes gave relatively similar tendency for the fission cross section when the target nucleus is in its excited state. At low energies (below 1 MeV), the calculated fission cross section for the first excited state is larger than that for the ground state, and the difference becomes smaller at higher energies. This observation is consistent with the phase-space argument; low energy reactions are strongly constrained by the spin selection rule.

## ACKNOWLEDGMENTS

This work was carried out under the auspices of the National Nuclear Security Administration of the US Department of Energy at Los Alamos National Laboratory under Contract No. DE-AC52-06NA25396.

[1] T. Rauscher and F.-K. Thielemann, At. Data Nucl. Data Tables **75**, 1 (2000).
[2] M. Arnould, Astron. Astrophys. **19**, 92 (1972).
[3] S. A. Karamian, C. B. Collins, J. J. Carroll, J. Adam, A. G. Belov, and V. I. Stegailov, Phys. Rev. C. **59**, 755 (1999).
[4] O. Roig, G. Belier, V. Meot, D. Abt, J. Aupiais, J. M. Daugas, C. Jutier, G. LePetit, A. Letourneau, F. Marie, and C. Veyssiere, Phys. Rev. C **74**, 054604 (2006).
[5] R. B. Firestone, *Table of Isotopes,* 8th ed. (Wiley & Sons, New York, 1998).
[6] W. Hauser and H. Feshbach, Phys. Rev. **87**, 366 (1952).
[7] T. Tamura, Rev. Mod. Phys. **37**, 679 (1965).
[8] G. R. Satchler, *Direct Nuclear Reactions* (Oxford University Press, Oxford, 1983).
[9] D. G. Madland, "Neutron Scattering by Nuclei Existing in Excited States: Preliminary Results," Los Alamos National Laboratory Report LA-UR-83-988 (1983).
[10] D. G. Madland and G. D. Doolen, "Neutron Scattering by Nuclei Existing in Excited States," Lawrence Livermore National Laboratory Report LLNL-CONF-8409220 (1985).
[11] P. Möller, J. R. Nix, W. D. Myers, and W. J. Swiatecki, At. Data Nucl. Data Tables **59**, 185 (1995).
[12] P. A. Moldauer, Phys. Rev. **123**, 968 (1961).
[13] P. A. Moldauer, Phys. Rev. C **11**, 426 (1975); **12**, 744 (1975); **14**, 764 (1976).
[14] P. A. Moldauer, Nucl. Phys. **A344**, 185 (1980).
[15] H. M. Hofmann, J. Richert, J. Tepel, and H. A. Weidenmüller, Ann. Phys. **90**, 403 (1975).
[16] J. J. M. Verbaarschot, H. A. Weidenmüller, and M. R. Zirnbauer, Phys. Rep. **129**, 367 (1985).
[17] S. Igarasi, in *Proceedings of the International Conference on Nuclear Data for Science and Technology, Jülich, Germany, 13–17 May 1991*, edited by S. M. Qaim (Springer-Verlag, Berlin, 1992), p. 903.
[18] S. Hilaire, Ch. Lagrange, and A. J. Koning, Ann. Phys. **306**, 209 (2003).
[19] M. Kawai, A. K. Kerman, and K. W. McVoy, Ann. Phys. **75**, 156 (1973).
[20] G. R. Satchler, Phys. Lett. **7**, 55 (1963).

[21] C. A. Engelbrecht and H. A. Weidenmüller, Phys. Rev. C **8**, 859 (1973).
[22] P. A. Moldauer, Phys. Rev. **135**, B642 (1964).
[23] H. Nishioka, H. A. Weidenmüller, and S. Yoshida, Ann. Phys. **193**, 195 (1989).
[24] T. Kawano, L. Bonneau, and A. Kerman, in *Proceedings of the International Conference on Nuclear Data for Science and Technology, Nice, France, 22–27 April 2007*, edited by O. Bersillon, F. Gunsing, E. Bauge, R. Jacqmin, and S. Leray (EDP Sciences, Les Ulis, France, 2008), p. 147.
[25] M. Ernebjerg and M. Herman, in *Proceedings of the International Conference on Nuclear Data for Science and Technology*, *Santa Fe, September 26–October 1, 2004*, edited by R. C. Haight, M. B. Chadwick, T. Kawano, and P. Talou, AIP Conf. Proc. No. 769 (AIP, New York, 2005), p. 1233.
[26] E.-I. Esch, R. Reifarth, E. M. Bond, T. A. Bredeweg, A. Couture, S. E. Glover, U. Greife, R. C. Haight, A. M. Hatarik, R. Hatarik, M. Jandel, T. Kawano, A. Mertz, J. M. O'Donnell, R. S. Rundberg, J. M. Schwantes, J. L. Ullmann, D. J. Vieira, J. B. Wilhelmy, and J. M. Wouters, Phys. Rev. C **77**, 034309 (2008).
[27] M. Jandel, T. A. Bredeweg, E. M. Bond, M. B. Chadwick, R. R. Clement, A. Couture, J. M. O'Donnell, R. C. Haight, T. Kawano, R. Reifarth, R. S. Rundberg, J. L. Ullmann, D. J. Vieira, J. B. Wilhelmy, J. M. Wouters, U. Agvaanluvsan, W. E. Parker, C. Y. Wu, and J. A. Becker, Phys. Rev. C **78**, 034609 (2008).
[28] *Handbook for Calculations of Nuclear Reaction Data, RIPL-2, Reference Input Parameter Library-2*, IAEA-TECDOC-1506, International Atomic Energy Agency (2006).
[29] A. Gilbert and A. G. W. Cameron, Can. J. Phys. **43**, 1446 (1965).
[30] T. Kawano, S. Chiba, and H. Koura, J. Nucl. Sci. Technol. **43**, 1 (2006).
[31] J. Kopecky, and M. Uhl, Phys. Rev. C **41**, 1941 (1990).
[32] S. F. Mughabghab, *Atlas of Neutron Resonances, Resonance Parameters and Thermal Cross Sections, $Z = 1$–100* (Elsevier, Amsterdam, 2006).
[33] L. Bonneau, T. Kawano, T. Watanabe, and S. Chiba, Phys. Rev. C **75**, 054618 (2007).
[34] Xia Yijun, Yang Jingfu, Yang Zhihua, Zhao Wenrong, and Yu Weiziang, Chinese J. Nucl. Phys. **10**, 102 (1988); **11**, 75 (1989).
[35] Xu Haishan, Xiang Zhengyu, Mu Yunshan, Chen Yaoshun, Liu Jinrong, and Li Yexiang, Chinese J. Nucl. Phys. **9**, 127 (1987).
[36] S. Joly, J. Voignier, G. Grenier, D. M. Drake, and L. Nilsson, Nucl. Sci. Eng. **70**, 53 (1979).
[37] R. C. Block, G. G. Slaughter, L. W. Weston, and F. C. Vonderlage, in *Proceeding of the Conference on Time-of-Flight Methods, Saclay, France, 24–27 July 1961* (European Atomic Energy Community, Brussels, 1961), p. 203.
[38] J. H. Gibbons, R. L. Macklin, P. D. Miller, and J. H. Neiler, Phys. Rev. **122**, 182 (1961); R. L. Macklin, J. H. Gibbons, and T. Inada, *ibid.* **129**, 2695 (1963).
[39] A. Koning and J.-P. Delaroche, Nucl. Phys. **A713**, 231 (2003).
[40] P. G. Young, "Experience at Los Alamos with use of the Optical Model for Applied Nuclear Data Calculations," Los Alamos National Laboratory Report LA-UR-94-3104 (1994).
[41] P. G. Young, E. D. Arthur, and M. B. Chadwick, "Comprehensive Nuclear Model Calculations: Introduction to the Theory and Use of GNASH Code," Los Alamos National Laboratory, LA-12343-MS (1992).
[42] J. E. Lynn and A. C. Hayes, Phys. Rev. C **67**, 014607 (2003).
[43] J. E. Lynn, in *Proceedings of the International Conference on Nuclear Data for Science and Technology, Santa Fe, September 26–October 1, 2004*, edited by R. C. Haight, M. B. Chadwick, T. Kawano, and P. Talou, AIP Conf. Proc. No. 769 (AIP, New York, 2005), p. 1193.